Metastability of the segregation-reversal composition profile at the $Pt_xNi_{1-x}(110)$ surface: A low-energy electron-diffraction study

Y. Gauthier, R. Baudoing, and J. Jupille*
Laboratoire de Spectrométrie Physique, Boîte Postale 87, 38402 Saint-Martin-d'Hères CEDEX, France
(Received 24 January 1989)

A low-energy electron-diffraction study of the surface segregation at $Pt_{10}Ni_{90}(110)$ is presented. The Pt concentrations in the first and second layers are, respectively, 6 and 52 at. %. The corresponding interlayer spacings differ from the bulk values by -4.5% and $+3.6\%$. This oscillating behavior is similar to that reported previously for $Pt_{50}Ni_{50}(110)$, the most spectacular result being that the segregation is also reversed with respect to the (111) face. Our results are discussed in the light of theoretical models which predict Pt segregation for Ni-rich alloys, Ni segregation for Pt-rich alloys, and a metastable situation in the range 30–60 at. %. We also discuss the influence, on chemical reactivity, of (i) the segregation reversal, (ii) the strong Pt enrichment in the second layer, and (iii) the two-dimensional ordering tendency.

I. INTRODUCTION

Surface alloys as well as surfaces of bulk alloys are a subject of great interest: on fundamental grounds, segregation mechanisms are still to be understood quantitatively for a class of potentially important alloys, and on technical grounds, many applications like catalysis by metallic particles or multilayered metallic structures require a good understanding of the segregation behavior at surfaces or interfaces.

Very few alloy surfaces are well known in detail: one of them, Pt-Ni has been extensively studied recently in the solid-solution phase. The (111) surface[1,2] is found to exhibit a systematic behavior: whatever the bulk concentration is, the composition profile is oscillatory with a Pt enrichment in the top layer (C_1) followed by a Pt depletion in the second layer (C_2) and a slight enrichment in the third one (C_3). The largest oscillation is found in the range 10–50 at. % Pt bulk concentration, and is accompanied by enhanced catalytic properties[3] and modified reactivities.[4]

The (110) face of the $Pt_{50}Ni_{50}$ alloy has been shown recently[5] to exhibit a total segregation reversal as compared to the (111) face. The top layer is found to be almost pure nickel, while the second layer is almost pure platinum, the oscillation being damped out only at the fifth layer. This extreme sensitivity of the segregation phenomena to the face orientation, in the case of Pt-Ni, has called for theoretical models.

Two theoretical studies of the segregation profile have been reported[6,7] which concluded to a relatively satisfactory picture for the (111) face. However, the (110) face was not quantitatively accounted for but a complex behavior was suspected: the tight-binding Ising model[6] (TBIM) concluded to a reversal with the bulk composition (Pt enrichment for Ni-rich alloys but Pt depletion for Pt-rich alloys). The embedded-atom method[7] (EAM) predicted the occurence of a metastable state in the range of Pt bulk concentration $C_b = 30$ to 60 at. %: one "branch" exhibiting Pt enrichment $C_b = 0$ to 60 at. % and the other branch exhibiting the observed segregation reversal $C_b = 30$ to 100 at. %. Experimentally, only one point lying on the Ni-rich branch was known and a central question was thus to investigate the segregation on the nickel side, where the Pt-rich branch is expected: it was decided to study $Pt_{10}Ni_{90}(110)$.

This is the topic of the present paper which is organized as follows: Sec. II reports on the experimental aspects, Sec. III deals with the low-energy electron-diffraction (LEED) analysis (structural and composition parameters), while Sec. IV discusses the present results against the predictions of the above models with some possible consequences in terms of reactivity and finally suggests some new investigations.

II. EXPERIMENT

All experiments have been carried out in an experimental setup consisting mainly of an ultrahigh vacuum (UHV) stainless-steel chamber, equipped with an ion gun and a two-grid system used for both LEED and Auger-electron spectroscopy (AES). A detailed description has been given previously.[8] The half-sphere-shaped grids and screen of the device allows beam intensities to be measured in the entire half-space above the crystal, for any incidence direction. Incidence, polar, and azimuthal angles can be set up within an accuracy of 0.1°. The sample is heated by electron bombardment and the temperature is measured by means of a (W–5 at.% Re)/(W–26 at.% Re) thermocouple fixed on the surface. The working pressure is in the 10^{-10} Torr range. The partial pressure of contaminant gases was kept very low owing to a titanium sublimation device, maintained at liquid-nitrogen temperature during the whole period of cleaning and data collection.

The $Pt_{10}Ni_{90}$ sample was cut to within less than 0.2° of the required (110) plane, out of a Pt-Ni single crystal rod having a nominal bulk concentration of 10 at. % plati-

num, x-ray analysis showing a lattice parameter in agreement with the tabulated value,[9] 3.572 Å (bulk interlayer spacing: 1.263 Å) which was used in the calculations. Once mounted in UHV conditions, the crystal was first cleaned by repeated argon ion bombardments and annealings at 1200 K in vacuum, until the AES spectrum was checked to be free of contaminants and the LEED $I(V)$ curves were reproducible (the latter criterium proved to be more relevant and constraining than Auger analysis). After this preliminary treatment, a 20-min argon bombardment followed by a 5-min annealing at 1070 K was sufficient to meet appropriate working conditions, before collecting data. Though it has been proved that no ordered phase is formed in the Pt-Ni alloy around 10 at. % platinum, it was checked by x rays that the above treatment resulted in the solid-solution phase, as expected from a recently published phase diagram.[10]

Observed by LEED, the crystal displayed a pattern with sharp spots (Fig. 1) typical of a clean fcc (110) surface. In addition, within large energy ranges, halfway between the [100] rows of the (1×1) structure, the diffraction diagram showed dim continuous streaks in the [100] direction, indicative of a tendency to (1×2) atomic arrangement, which occasionally turned into diffuse spots ordered as for a $c(2\times2)$-like superstructure. The presence of contaminants being unambiguously discarded by AES analysis, the additional features were attributed to a tendency to chemical ordering of the alloy surface, comparable to that observed on $Pt_{10}Ni_{90}(111)$ (see discussion in Sec. IV D 2). Tentatively, we tried to better organize this two-dimensional (2D) ordering: the crystal was annealed for longer and longer periods (up to 4 h) at 900 °C but these cycles did not change the appearance of the LEED pattern. This partial ordering seems the most stable situation for this alloy. However, these extra features showed intensities which were mostly lying more than an order of magnitude lower than the intensities of the main (1×1) spots. The decision was thus made to take only into account these latter spots and to neglect the former ones. A full understanding of this partial ordering falls within the ability of diffuse LEED, but, nevertheless, a tentative interpretation is proposed in Sec. IV.

The data collection was computer controlled and beam intensities were recorded at energies ranging from 30 to 280 eV, in steps of 1 eV, at normal incidence and at a po-

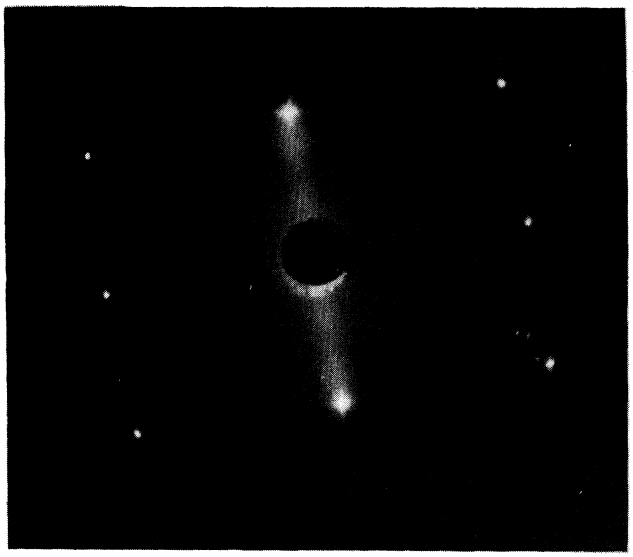

FIG. 1. Typical LEED pattern from $Pt_{10}Ni_{90}(110)$ close to normal incidence (see text). The spots correspond to the bulk periodicity. Additional weak streaks are visible along the [100] direction. (The small spurious satellites are artifacts due to reflection in the glass screen.)

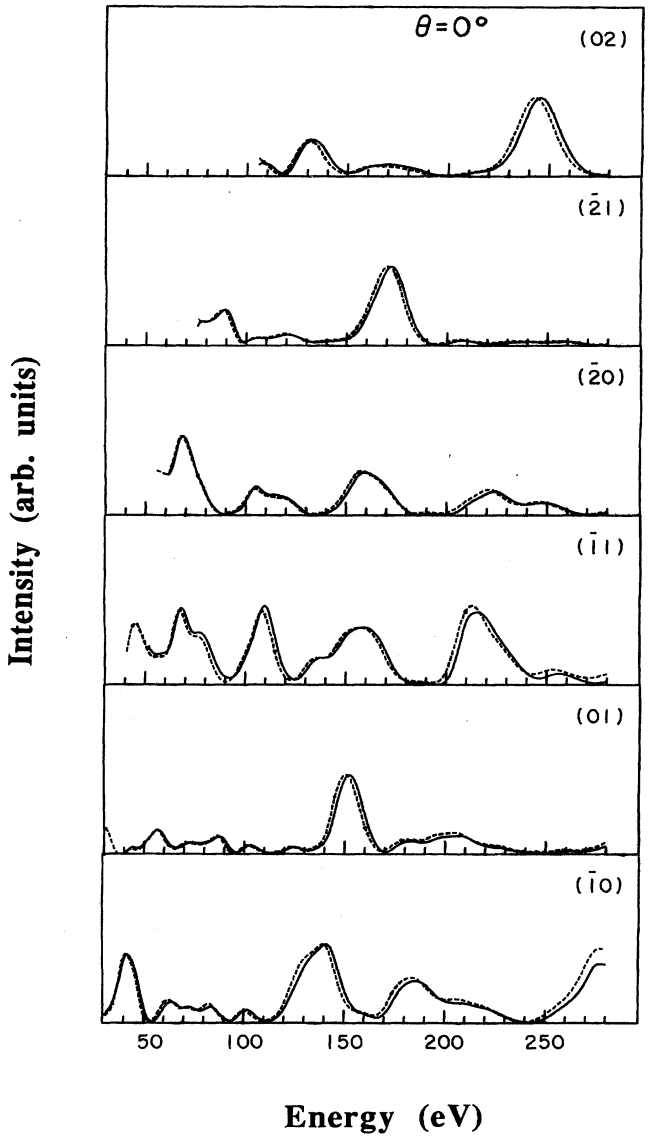

FIG. 2. $Pt_{10}Ni_{90}(110)$ normal incidence measured spectra. The solid and dashed lines denote spectra recorded at two different places on the sample and illustrate a very good reproducibility. Beam indices are indicated in the upper-right corner of each panel.

lar angle of 20° along the [100] azimuth. The symmetrically equivalent beam intensities proved very similar. They were, however, averaged to yield even better data, leading to six and twelve nonequivalent $I(V)$ curves for the normal and the oblique incidence, respectively. After background substraction the spectra were normalized to constant incident current. Reference data—incident current, AES spectra, and LEED intensities—were recorded to control any drifting that could occur during the process. As the specular beam intensity showed no detectable change, the influence of carbon contamination which was occasionally detected at a very low level (<0.05 monolayer) was considered as sufficiently low to be neglected. Moreover, normal incidence spectra were recorded on two different locations on the sample in order to control the homogeneity of the surface concentration profile. The two sets of $I(V)$ curves (Fig. 2) appear very similar apart from some very tiny shifts in peak positions and relative intensities. From our own experience, no influence could be suspected from visual inspection, but both sets were however considered in the analysis.

III. LEED ANALYSIS

A. On the calculations

A layer-by-layer Korringa-Kohn-Rostoker (KKR) program fitted with a layer-doubling routine (LDM) was employed for the LEED calculation.[11,12] High Pt content coupled with small interlayer distances (≤ 1 Å) made compulsory a check of convergence in the LDM stacking in the case of $Pt_{50}Ni_{50}(110)$.[5] In the present study, the bulk Pt concentration is much smaller, and visual comparison of LEED spectra with corresponding ones of Ni(110) (Ref. 13) allowed us to conclude qualitatively to an overall low-Pt concentration in the selvedge. Moreover, on Ni(110), the contraction of the first interlayer distance is much smaller than that of $Pt_{50}Ni_{50}(110)$, (-8% instead of -19%). As a consequence, *a posteriori* confirmation is given by our final conclusions, we estimated LDM could be used safely for the surface under analysis.

Assuming a random occupation of the lattice sites, the Pt-Ni alloy can be represented by averaged nickel-platinum scatterers, each surface layer being given its particular concentration.[1,2,5] At each layer, the LEED scattering amplitudes are calculated within the averaged-t-matrix approximation (ATA),[14] since the sliced ATA fits in with the KKR approach. The scattering amplitudes are derived from linear muffin-tin orbital (LMTO) potentials and platinum is treated relativistically.[5] Up to ten phase shifts were included in the whole course of the study. The inner potential $V_R(E)$, which is energy dependent, is assumed to be identical for all layers and is allowed to be shifted rigidly by ΔV_R, as usual in LEED. The absorptive potential, $V_i(E)$, and the Debye temperature were given the values used in previous works.[1,2,5]

B. Parameters

The principle of the search for a surface structure consists in fitting the parameters of a structural model, sampling narrower and narrower areas centered around the estimated best solution by means of denser and denser grids. The model involves a bulk having the nominal platinum concentration, topped by surface layers whose parameters C_i (platinum concentration of layer i) and $d_{i,i+1}$ (interlayer distance between the ith and the $(i+1)$th layer), $i=1,2,3$, are allowed to vary, as well as the inner potential shift ΔV_R. The curves resulting from LEED calculations are compared to experimental data via five different metric distances for which a full description has been given previously:[15] $D1$, $D2$, $D4$, $D2y$, $D4y$. The metrics $D2y$ and $D4y$ were included in the last step of the analysis only. All the combinations of parameters which can be obtained within the framework of the chosen grids are systematically examined against each metric distance as to minimize it and do determine the best set of parameters.

C. Search for an optimum model

The LEED analysis was performed in three successive steps. In the first step, we restrict ourselves to normal incidence data to find out approximately what the segregation profile is, covering the whole range of concentration for the two outermost surface layers. The crystal is assumed to be bulklike from the third layer on and we use the loose grids of Table I for the concentrations C_1 and C_2. According to the usual behavior of the fcc (110) metal faces[13] and to the similarity between Ni(110) and $Pt_{10}Ni_{90}(110)$ spectra, the first interlayer spacing was sup-

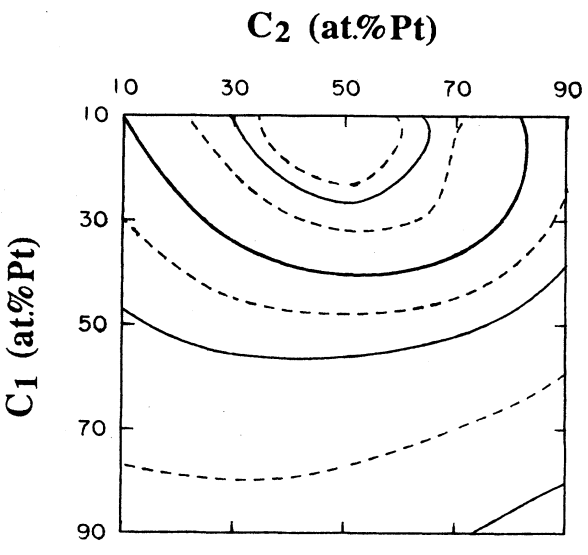

FIG. 3. Metric distance D_1 contour plot, for normal incidence data, showing a unique minimum in the C_1-C_2 space. The relaxations Δd_{12} and Δd_{23} are fixed at near-optimum values. The levels have been chosen according to $[D_{\min}+(D_{\max}-D_{\min})\times 2^n/100]$. $D_{\max}$ and $D_{\min}$ denote the maximum and minimum value of the metric distance in the whole range of parameters.

TABLE I. Preliminary model of $Pt_{10}Ni_{90}(110)$ determined by LEED and metric distances. Normal-incidence data only. The optimum parameter values are taken directly from the grid and not interpolated.

Metric (%)	C_1 (at. %)	C_2	Δd_{12} (% of d_{bulk})	Δd_{23}	ΔV_R (eV)
			Step 1		
Grid	10(20)90	10(20)90	−19(3)+1	−4(2)+8	−3(1)3
$\langle D \rangle$	10–30	50	7	3	1
			Step 2		
Grid	00(10)50	30(10)70	−12(2)−2	−2(2)+6	−3(1)3
$D1=14.0$	10	50	−6	2	1
$D2=4.2$	10	50	−6	0	−1
$D3=8.7$	10	50	−6	2	3

posed to be contracted. The relative relaxation Δd_{12} was varied from +1% to −19%, the latter being the large value found for $Pt_{50}Ni_{50}(110)$.[5] Likewise, it was assumed that the multilayer relaxation is attenuated towards the bulk. The first step led to the following crude estimates of the parameters under study: $C_1=10$ to 30 at. % Pt, $C_2=50$ at. % Pt, $\Delta d_{12}=-7\%$, and $\Delta d_{23}=3\%$. The examination of the (C_1,C_2) charts associated to the three metric distances, $D1$,$D2$,$D4$, *proved the minimum to be unique throughout the entire* C_1-C_2 *space,* as illustrated in Fig. 3 for the metric $D1$.

As we kept on optimizing the metrics solely against the set of spectra recorded at normal incidence, we defined a second set of shorter grids. In addition, the relaxation between the third and fourth layers was allowed to vary. As evident from Table I the optimized values, not interpolated, are very consistent from one metric to the other and are very close to those of the previous step. The grids to be used in the final calculations were logically deduced from these estimates (see Table II). The final optimization was based on the entire set of experimental $I(V)$ curves, which involved six spectra recorded at normal incidence and twelve spectra at 20° incidence along the [100] azimuth. The result of the LEED analysis is reported in Table II for five metrics (for the two experimental normal incidence data sets, we do get exactly the same answer, which is not surprising in view of the very good agreement of the data, shown in Fig. 2). The geometrical parameters and concentrations are averaged over the metrics and the standard deviations follow from the dispersion among metrics. All five metrics end with quite small figures, equivalent to what came out from our previous studies of the same alloy[1,2,5] and are significantly of a good level of agreement. Cuts in the parameter space are illustrated for the metric $D1$ in Figs. 3–5. In the (C_1,C_2) plane, the metric shows equal sensitivity to both concentrations (Fig. 4), while the sensitivity is much larger to the interlayer spacing than to the concentration

TABLE II. Surface segregation and multilayer relaxation on $Pt_{10}Ni_{90}(110)$ by metric optimization on 18 spectra at normal and off-normal incidence. Average and standard deviations refer to metrics. Grid: $C_1=0(5)20$ at. %, $C_2=30(10)70$ at. %; $\Delta d_{12}=-8(1)-4\%$; $\Delta d_{23}=-2(1)+6\%$; $\Delta d_{34}=-3(1.5)+3\%$; $\Delta V_R=-2(1)4$ eV.

Metric (%)	C_1 (at. %)	C_2	Δd_{12} (% of d_{bulk})	Δd_{23}	Δd_{34}	ΔV_R (eV)
$D1=13.32$	7	51	−5.4	3.3	0.5	1.9
$D2=3.94$	12	52	−4.9	5.5	−0.5	2.5
$D2y=2.67$	2.5	56	−4.0	3.0	0.8	2.0
$D4=7.99$	6	51	−4.7	3.6	−0.5	3.5
$D4y=4.77$	4.5	51.5	−3.7	2.8	0.5	3.5
			Result			
Average	6.4	52.3	−4.5	3.6	0.2	2.7
standard deviation	3.6	2.1	0.7	1.1	0.6	0.8

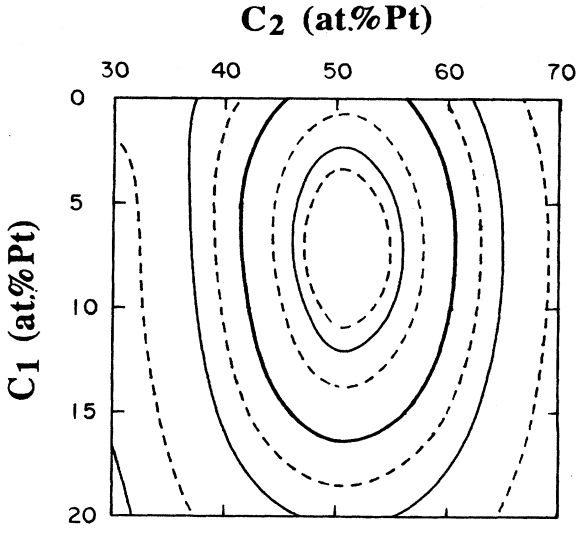

FIG. 4. Same as Fig. 3 for the overall set of data (normal plus oblique incidence) in a restricted range of concentration C_1-C_2, around the minimum of Fig. 3.

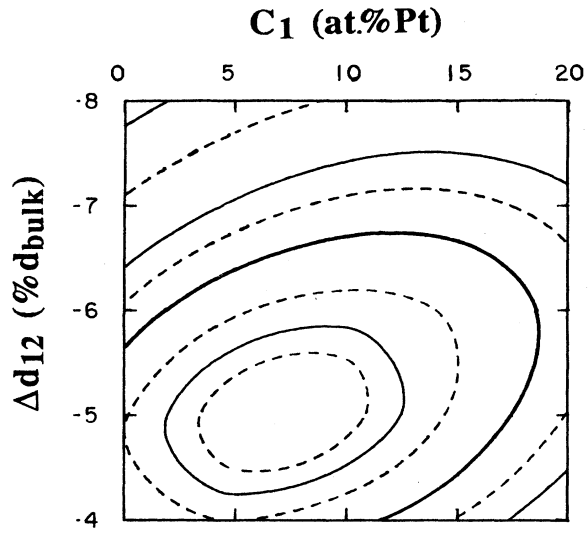

FIG. 5. Same as Fig. 4 in the Δd_{12}-C_1 space.

(Fig. 5), which is consistent with the findings of our previous studies. In both figures, a unique and well-defined minimum appears. A visual comparison of experimental and theoretical spectra, for the optimized structure, clearly confirms the goodness of the fit (Fig. 6). Moreover the spread among metrics is very small, giving us good confidence that we are now very close to the best model.

The first layer is almost pure nickel with only 6.4 at. % (less than the bulk content, 10%) while the second layer is strongly enriched, $C_2 = 52.3$ at. %. The standard deviation appears to be larger for C_1, the top-layer concentration, than for C_2. This slightly less good precision on C_1 can probably be attributed to the smaller overall scattering cross section of Pt as compared to Ni, due to much smaller Pt content in C_1 than in C_2.

The multilayer relaxation turns out to be alternating, starting with a contraction ($\Delta d_{12} = -4.5\%$) followed by a slight expansion and vanishes on the third layer. This behavior is similar to what has been established for a number of (110) fcc metallic surfaces.[13] One would expect relaxations intermediate between that of $Pt_{50}Ni_{50}$(110) (Ref. 5) and Ni(110).[13] In fact, the first relaxation, -4.5%, happens to be rather small compared to the strong contraction, -19%, found on $Pt_{50}Ni_{50}$(110) but also smaller than that of Ni(110), -8%. It is also worth mentioning that the relaxation attenuation is weaker: for the above-mentioned surfaces, the absolute value of Δd_{23} is about one-half of Δd_{12} while in the present case, the damping is less pronounced. Considering hard-sphere radii from

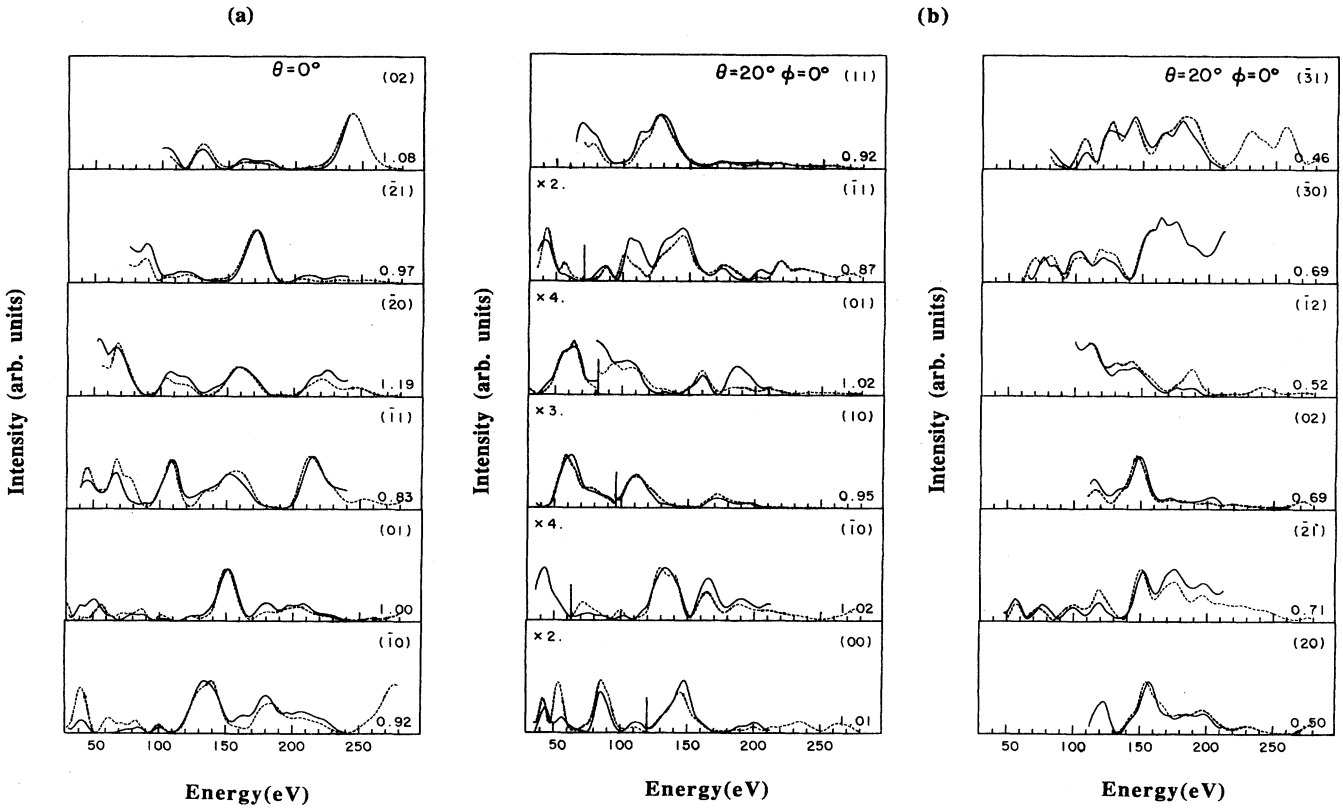

FIG. 6. Beam spectra from $Pt_{10}Ni_{90}$(110) for near-optimum parameters. (a) Normal incidence and (b) oblique incidence. Calculation (solid line); experiment (dashed line).

Pearson's handbook[9] and using the optimum concentrations of Table II, the crystal would exhibit, from the first layer and inwards, 1% contraction and 9.6% expansion, i.e., very different from the actual situation. In conclusion, *the measured geometrical relaxations follow from strong relaxation of interatomic bonds.*

A last comment concerns the concentration on the third layer. Owing to the large value of C_2, it would not be strange that the concentration oscillation propagate deeper into the crystal. An attempt was made to optimize the concentration within the third surface layer. The concentration of the two top layers were set at near optimum values, 10 and 50 at. % Pt, respectively, and C_3 was varied from 0 to 50 at. %. The best fit could be located in the range $0 \leq C_3 \leq 20$ at. % Pt, though the limit of the resolution of the analysis was reached.

IV. DISCUSSION

A. Oscillation-segregation reversal: Face-dependent composition profile

Segregation profiles are known for four different surfaces of Pt-Ni alloys[1,2,5] and a comparison of general trends is enlightening. In particular, the composition profile, $(C_1, C_2) = (6, 52)$, of the present work resembles that of $Pt_{50}Ni_{50}(110)$,[5] $(C_1, C_2) = (0, 95)$: the concentration oscillates with a large amplitude, and the second layer is strongly enriched with Pt, while C_1 is less than the bulk value.

The oscillation appears to be the rule since three studied (111) faces of Pt_xNi_{1-x} ($x = 0.78, 0.5, 0.10$) (Refs. 1 and 2) exhibit the same trend. The most striking feature is the segregation reversal from the (111) to the (110) surfaces. The formers terminate with a Pt-rich top layer and a Ni-rich second layer while the latters terminate with a Ni-rich top layer and a Pt-rich second layer.

Although oscillations are known at Ag-Au alloys[16] for instance, the Pt-Ni alloy is the first one for which face related segregation reversal has been reported. Such a behavior is a clear warning on the limits of studies on polycrystalline samples.

B. Ability of LEED plus ATA to distinguish among models

In the next section we are concerned with the segregation profile of $Pt_xNi_{1-x}(110)$ as a function of the bulk concentration and this profile is discussed in the light of theoretical predictions. *The relevance of the following discussion depends on the reliability of the concentration at surfaces determined by LEED, and it is quite important to illustrate to which point LEED coupled with ATA is able to distinguish among different sets of concentration,* (C_1, C_2). To emphasize how great the sensitivity of LEED spectra is with respect to changes in the surface composition, we show, in Fig. 7 the $I(V)$ curves for three relevant concentration profiles: (i) $(C_1, C_2) = (10, 10)$ which corresponds to a simple truncated bulk; (ii) $(C_1, C_2) = (50, 10)$ as suggested for $Pt_{50}Ni_{50}(110)$ by theoretical calculations with EAM (Ref. 17), and (iii)

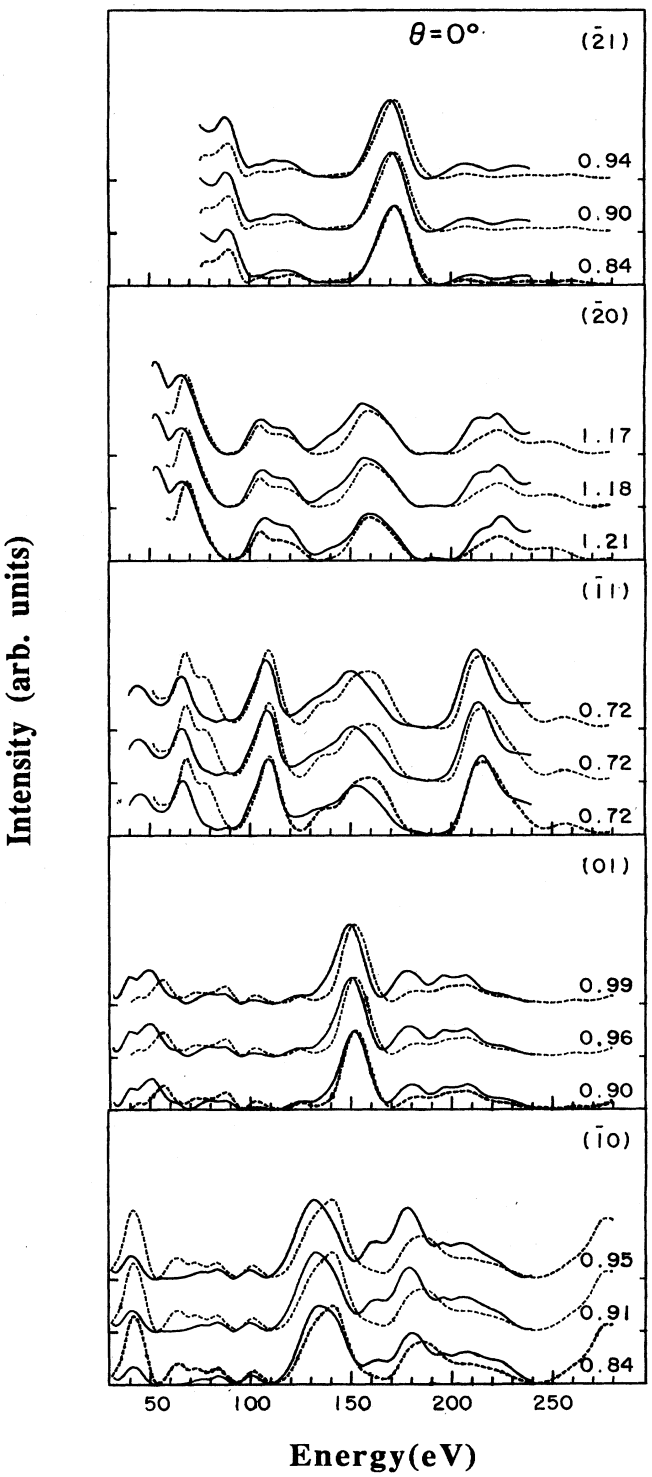

FIG. 7. Sensitivity of normal incidence calculated spectra (solid line) to changes in the concentration profile, in comparison with experimental spectra (dashed line) for near-optimum relaxations: $\Delta d_{12} = -6\%$, $\Delta d_{23} = 3\%$. In each panel we show three significant theoretical models: (a) $C_1 = 10\%$, $C_2 = 10\%$ (truncated bulk), bottom curve; (b) $C_1 = 10\%$, $C_2 = 50\%$ (near-optimum solution at normal incidence), middle curve; (c) $C_1 = 50\%$, $C_2 = 10\%$ [prediction of TBIM (Ref. 6) and EAM (Ref. 7)] top curve.

$C_1C_2=(10,50)$, the node of the first grid used herein which lies closest to our final conclusion. Relaxations and inner potential shifts are those obtained for the best fit (Table I). As they are actually significant of the whole data set, four beams measured at normal incidence are presented.

The $(C_1,C_2)=(50,10)$ model, prediction of EAM, clearly shows the worst agreement with measured spectra and can be readily discarded. The $(C_1,C_2)=(10,10)$ model leads to rather big discrepancies with experimental curves compared to $(C_1,C_2)=(10,50)$. This is particularly true for the $(\bar{1}\,1)$ and $(\bar{1}\,0)$ beams. This clearly demonstrates that even changes in the second-layer composition substantially modify the calculated spectra. Thus, although the fit relies on metric distances, the general trends can be unambiguously drawn from a visual inspection. At last, it has to be said that additional confirmation follows from angular Auger experiments which yield the same oscillation.[18]

C. (110) face and metastability

Segregation at alloy surfaces has long since focused the attention of scientists and a number of theories have been proposed to explain or predict the composition profiles. They turned out to be successful for a wide class of alloys except for some of them, unfortunately of large practical importance like Pt-Ni and Pt-Fe, for example.[19] Among these predictions, we consider two of them which recently could account for the actual situation at $Pt_xNi_{1-x}(111)$ surfaces and are relevant to this paper: the embedded-atom method[7] and the tight-binding Ising model.[6] All other empirical theories are set aside as unable to correctly describe the Pt-Ni system for different face orientations.

1. Summary of LEED results

The present results are reported in Fig. 8 together with our previous conclusions on $Pt_{50}Ni_{50}(110)$. The concentration in the first and second layers are drawn versus the bulk composition. The predictions of the EAM and TBIM models are recalled also in Fig. 8.

(i) Let us first emphasize that *the limit at 100 at. % Pt concentration is badly accounted for;* indeed, Pt(110) reconstructs with a (1×2) superstructure interpreted as a missing-row geometry. *There is thus a singularity in the concentration profile, $(C_1,C_2)=(50,100)$, at the pure Pt side of $Pt_xNi_{1-x}(110)$.* A crucial point, especially, is the limit beyond which the alloy reconstructs like pure Pt(110). It might be that the least Ni concentration is enough to relax strains and remove the reconstruction as is often the case with adsorbates: the C_1 profile would then be discontinuous at the Pt side.

(ii) *The main characteristic is the huge Pt enrichment in the second layer,* simultaneously with a very low Pt concentration in the outermost layer. As far as $Pt_xNi_{1-x}(110)$ is concerned, *such a trend agrees very well with the EAM calculations and could be explained within the framework of TBIM* provided the segregation reversal it predicts is shifted towards low-Pt bulk concentration by a large amount.

(iii) *In contrast, the predictions for $Pt_{10}Ni_{90}(110)$ are reversed with respect to the experimental data.* Although the oscillation comes out from the calculation, the surface sandwich yields a rather rich top layer, $(C_1,C_2)=(50,5)$.

2. Pt segregation for dilute Pt alloy

The experimental data seem to show, in fact, that C_1 is lower than the bulk concentration in the whole range of

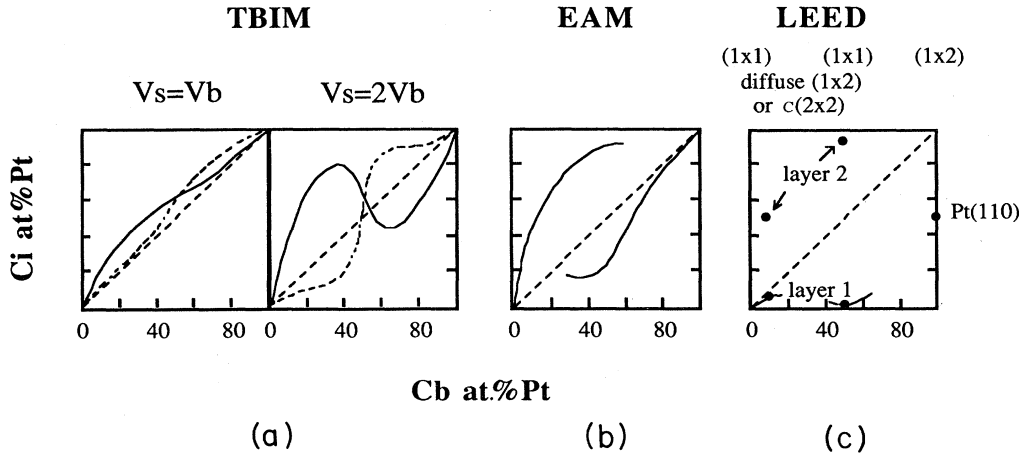

FIG. 8. Variation of the Pt concentration in the first (C_1) and second layer (C_2) as a function of the bulk concentration (C_b) for $Pt_xNi_{1-x}(110)$: C_1 (——), C_2 (— — —). (a) Results from TBIM (Ref. 6) for two different surface-pair-interaction potentials V_s. (b) Results from EAM. Two C_2 values only are known for $Pt_{10}Ni_{90}(110)$ (Ref. 17) and $Pt_{50}Ni_{50}(110)$ (Ref. 7). (c) Experimental results from this work and from Ref. 5. The corresponding LEED patterns are indicated at the top. Pt(110) reconstructs with a (1×2) pattern (missing-row model) with 50 at. % Pt sites in the top layer while on the alloy 100% sites are occupied.

concentration while reversal is expected theoretically. At the $Pt_{50}Ni_{50}(110)$ face, from LEED, the Pt concentration of the first layer is almost zero and, extrapolating the trend to $Pt_{10}Ni_{90}(110)$ would lead to probably less than 1%. However, C_1 is seen to increase from 0 to 6 at. % when the bulk concentration C_b decreases from 50 to 10 at. %. We do believe that the accuracy of both LEED analyses is sufficient to accept this increase as significant. It indicates a great modification of the Pt-Ni system behavior on the nickel side: *the actually observed concentration $C_1 = 6\%$ is of the same order of magnitude as that in the bulk, $C_b = 10\%$.* Although drastically reduced by comparison with the predictions, a tendency to segregation reversal versus the bulk composition is found. More precisely, one should speak of an "anomalous" increase of C_1 at low Pt content, as illustrated in Fig. 8(c), even though two surfaces only have been scrutinized. In that respect, it is remarkable that a similar behavior is expected and found for low-copper concentration Cu_xNi_{1-x} alloys,[20] as discussed in Sec. IV C 4.

3. *On the predictions*

It is probably too early to draw final conclusions and additional data are necessary to fill up the uncovered regions of Pt bulk concentration. Nevertheless the discrepancy remains still large between the LEED and EAM-TBIM results. Apart from the poorly pronounced increase of C_1, the discrepancy about C_2 has to be explained. Regarding EAM, one has to be aware that in the version developed by Lundberg,[7] only bulk properties are used for determining the parameters of the crystal and "if surface properties were introduced in a way to give accurate relaxations for the pure metals, we could expect an agreement within 1% for the relaxation of the alloy."

As to TBIM, two hypotheses deserve discussion. From the calculations, it appears that the C_1 profile versus C_b is the result of a subtle balance between a size effect (about 10% difference in Pt and Ni radii) and the pair-interaction terms. Precisely the size mismatch term is known for pure Pt and Ni for which the signs are different, but not for intermediate mixtures. For the alloy, the authors interpolate with a sine shape (see Fig. 1 of Ref. 21). This assumption has not been justified and, owing to the large change including the sign, might introduce spurious distortions in the final profiles. The solutions proposed for dilute concentrations are probably correct but are questionable in the medium concentration range. In particular, the point where C_1 reaches the bulk value [Fig. 8(b)] could be shifted in one or the other direction, depending on the actual weight of the size effect. Similarly, the surface pair interaction V_s is proved to very efficiently alter the shape of the profile.[6] From Fig. 2 of Ref. 22, the general shape of the pair-interaction potential versus the d-band filling is very similar for the bulk and for the different faces, and weakly dependent on C_b. However, dealing with a specific case, for instance a d-band filling of eight electrons, Fig. 9(a), or of 9.5 electrons, Fig. 9(b), V_s and/or V_b happen to *depend critically on C_b* and to vary in a wide range. In this discussion we

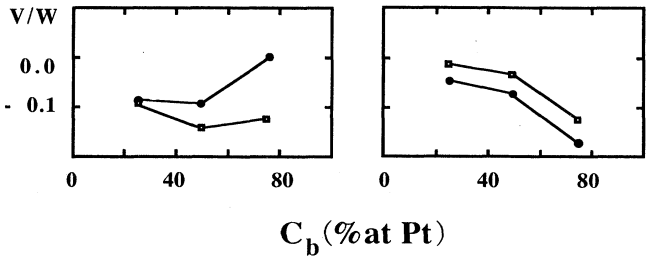

FIG. 9. Variation of the surface, V_s (circles), and bulk, V_b (squares), pair-interaction potential (scaled to the bandwidth W) as a function of the bulk concentration for a d-band filling nd: left panel, $nd = 8$ electrons; right panel, $nd = 9.5$ electrons.

have deliberately restricted our point to a constant d-band filling, but owing to the *great sensitivity* of V_s and V_b to this parameter, it is certainly a relevant task to study the local electronic properties of alloy surfaces in presence of large segregation effects.

4. *Segregation reversal and metastability*

Notwithstanding, it was emphasized that, within the EAM framework, multiple solutions to the segregation equations can occur, leading to two branches in the segregation profile versus C_b. One of the branches looks like the proposed behavior of TBIM [Fig. 8(a)]. The branch starting on the nickel side is called metastable, the stable state being the one observed in LEED, the two branches coexisting in the range $C_1 = 30$–60 at. %. The concept of metastability was used by Lundberg since there is quite a small energy difference from one branch to the other and since, in the free-energy map (C_1, C_2), a saddle point appears between the two minima. Till now, this metastable state (or rather a segregation reversal versus C_b) has not been observed throughout our studies or in other experimental works by ion-scattering spectroscopy (Ref. 23). In the case of Pt(110), two states have been observed: the stable one, where the surface is reconstructed with a (1×2) periodicity and a metastable (1×1) phase. As regards the alloy, the stable state corresponds to a nonreconstructed surface: the presence of two chemical species with different radii is probably at the origin of this difference between the pure metal and the alloy. However, the existence of a metastability shows up perhaps as a bump in the C_1 profile versus C_b. The parallel has to be made with very recent TBIM predictions by Legrand *et al.*[20] For the (110) face studied herein, they show that: two branches occur in the dependency of the surface concentration C_1 versus the bulk concentration, C_b (see Fig. 10); at low bulk Pt content, $10 \le C_b \le 50$ at. %, the surface enriches with Ni; at $C_b = 10\%$, there is a discontinuity in the surface concentration: slightly above $C_b = 10\%$, C_1 shows a tendency to increase and reaches the bulk value at $C_b = 10\%$. Below 10%, a marked Pt enrichment is predicted. For the surface studied by LEED so far, the general trends of TBIM predictions happen to be in close concordance with our results. One could wonder if such

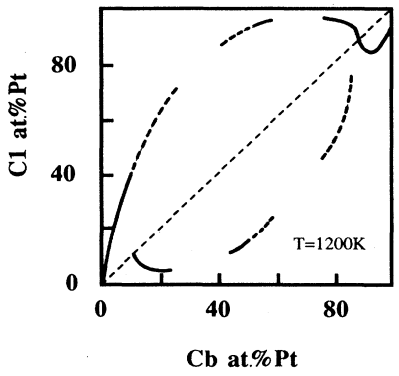

FIG. 10. $Pt_xNi_{1-x}(110)$: prediction of the TBIM model for the surface Pt concentration, C_1, as a function of the bulk concentration, C_b; (——) stable and (— — —) metastable state. Compare with the LEED results of Fig. 8(c).

a metastability has any incidence on the reactivity of the surface, or, in other words if, in the presence of some adsorbate, the alloy would behave as platinum surfaces and show structural instability:[24] during CO oxidation, the Pt(100) and Pt(110) surfaces reconstruct.

Finally we would like to emphasize that the *reconstruction of Pt(110) has not been taken into account,* which in turn is likely to produce perturbations in the composition profile on the very Pt-rich side. The additional pieces which we have brought to the overall comprehension of Pt-Ni alloys should help significantly *to better predict surface segregation* through a better knowledge of the *surface-pair interaction and size-mismatch contribution to the total energy.*

D. Surface composition and catalysis

The basic interest of bimetallic alloys is their use in catalysis to promote some specific products, and it is of first importance to improve the selectivity and activity for a number of reactions. Selectivity and activity obviously depend on the electronic arrangement at the surface and it is quite easy to understand that different geometries and/or composition in the top layer will lead to different chemical and catalytic properties.

1. Influence of face orientation and bulk composition

It has been demonstrated that the selectivity and activity can be modulated at the (111) face of Pt_xNi_{1-x} alloys by changing the bulk composition.[3,4] When C_b varies from 10 to 78 at. % Pt, the surface concentration increases from 30% to 99%, the geometry being almost the same but for the lattice parameter:[1,2] improved properties are found in the range $C_b = 10-50$ at. %. Similarly, the orientation greatly influences the catalytic behavior with respect to the hydrogenation of butadene into butenes: from the (111) to the (110) $Pt_{50}Ni_{50}$ surfaces the activity is improved by a factor of 11 (Ref. 25), which is really valuable on the economic point of view. A few more comments come in with the (110) orientation in the range $C_b = 10$ to 50%.

(i) In addition to variations in the lattice parameter with C_b, the vertical spacings vary in a wide range (−6% to −19% for Δd_{12}), from which one can expect possible changes in the surface electronic properties.

(ii) From our LEED results, the first layer is almost pure nickel, and the actual modification concerns C_2, which increases from 52% to 95%: C_2 can be tuned in a rather wide range and this effect is certainly not negligible.

(iii) Because the (110) face is open, atoms in the second layer become visible for small adspecies, C,H,O, etc. (for instance, S atoms on a Ni(110) surface are strongly bound to nickel atoms in the second layer[26]) and it is likely that the concentration in layer 2 plays a crucial role in monitoring the reactions. Detailed studies in the whole range of bulk concentration might help improving the already very good selectivity and activity of $Pt_{50}Ni_{50}(110)$.

2. Surface 2D ordering and active sites

Up to now, we have neglected the fact that we are dealing with substitutional alloys and we have discussed in terms of average layer composition. Let us assume that both species, Pt and Ni, are distributed at random as illustrated in Fig. 11(a), according to their optimum concentrations, $(C_1, C_2) = (6, 52)$. In layer 1, the majority sites, Ni atoms, are located above a layer containing very few "isolated" atoms (Pt atoms surrounded by Ni atoms or vice versa) but rather linear chains several identical atoms long. There are clearly several types of sites involving layers 1 and 2 leading to possibly different properties. These configurations can play a role in reactions as specific catalytic sites or by influencing the electronic densities at the top-layer atoms. The local environment might be crucial for molecules needing adjacent sites to be adsorbed and/or transformed.

In Sec. II, we have mentioned the presence of extra features in the elastic background, between the bulk spots: (i) streaks along the [001] direction corresponding to a (1×2) real space ordering: (ii) $c(2\times2)$-like broad spots appearing at only rare conditions. Since no contaminants could be detected, we are left with the assumption that partial ordering occurs. Two origins can be called for to explain the ordering: geometrical reconstruction such as the (1×2) missing-row model of Pt(110) or chemical ordering of Pt and Ni atoms. Such a structure, where 50% atoms are removed, would produce drastic changes in the integer-order beams—that we have considered in our calculations. This is clearly demonstrated by the differences in the spectra recorded on the (1×2) and (1×3) reconstructed Pt(110) surfaces.[27]

This seems far less probable than the other explanation, namely, chemical ordering in layers containing 100% atoms. The second layer just contains the amount $(C_2 = 52\%)$ necessary to produce (1×2) or $c(2\times2)$ superstructures. As such, it appears to be the probable origin of the weak-diffuse streaks rather than the first and third layers which contain very little Pt atoms. The streaks are elongated and continuous in the [001] direction but are rather narrow in the [110] direction. This means that in the latter, the atomic arrangement is al-

most periodic while disorder occurs in the former direction. In other words, the second layer can be viewed as a set of similar rows with a [110] orientation: these rows are made of alternating Pt and Ni sites giving rise to the (1×2) periodicity. However, stacking faults are very likely to occur from one row to the adjacent one and less frequently within the row itself as shown in Fig. 11(b). This distribution contains (1×2) unit cells as well as $c(2\times2)$ ones although less frequent. In contrast to the previous assumption (a totally random distribution in all layers), Pt and Ni atoms alternate along the [110] rows so that now, most Pt sites have only Ni first neighbors and vice versa. Roughly speaking, one type of Pt catalytic site is present in this case.

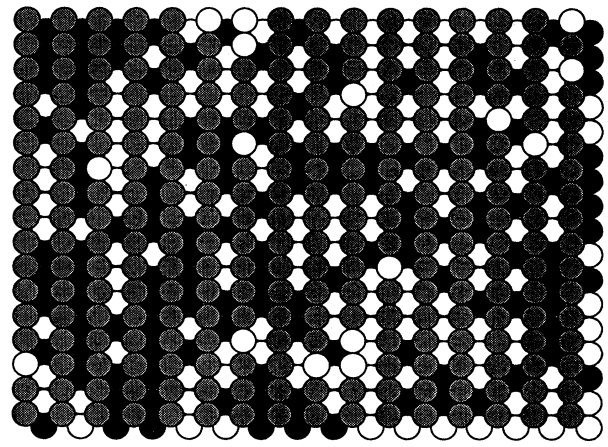

(a)

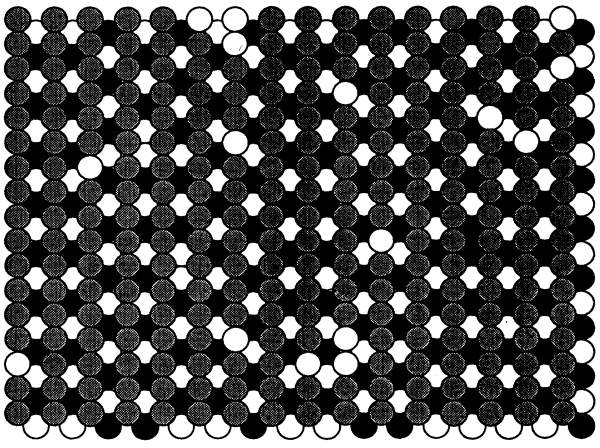

(b)

FIG. 11. $Pt_xNi_{1-x}(110)$: schematic real-space picture of surface layers having respective concentration $(C_1,C_2)=(6,52)$, corresponding to the optimum model. (a) Totally random distribution of species: small Pt and Ni aggregates and chains. (b) Partially ordered structure: high periodicity within rows in the [110] direction and random distribution of the rows in the [001] direction: white circles, Pt atoms in layers 1 and 2; grey, black circles, Ni atoms in layers 1 and 2, respectively.

The actual picture describing best the actual surface is more likely the structure of Fig. 11(b), but intermediate situations cannot be ruled out definitely. However, alternating species along the [110] rows lowers most probably the elastic energy associated to Pt enrichment in this second layer, as opposed to long chains of adjacent Pt atoms. A more detailed analysis of the extra features visible in the background is required but is out of the scope of this paper. In that regards, diffuse LEED might help to distinguish among the various possibilities. To conclude on this point, it seems that a direct comparison of substitutional and perfectly ordered crystals would probably bring in important pieces of information on the influence of 2D ordering in the context of catalysis.

V. SUMMARY

We have reported a LEED investigation of the segregation on the substitutionally disordered alloy $Pt_{10}Ni_{90}(110)$, as a crucial test of the occurrence of a metastable state at $Pt_xNi_{1-x}(110)$. The calculations are performed in the framework of the averaged t-matrix approximation, using a layer-by-layer program fitted with layer doubling for the LEED analysis and metric distances for spectra comparisons. We conclude that the concentration and interlayer spacing oscillate and are attenuated, from the surface and inwards, over three layers. The final parameters are

$$C_1=6.4\pm3.6 \text{ at. \%}, \quad d_{12}=1.206\pm0.09 \text{ Å},$$

$$C_2=52.3\pm2.1 \text{ at. \%}, \quad d_{23}=1.308\pm0.14 \text{ Å},$$

$$C_3=10\pm10 \text{ at. \%}, \quad d_{34}=1.265\pm0.09 \text{ Å}.$$

The segregation happens to be reversed with respect to the (111) face. These results make more general the tendency observed on $Pt_{50}Ni_{50}(110)$ which exhibits a well-defined Ni-Pt surface sandwich: the (110) face favors Ni enrichment contrary to the (111) face which enriches with Pt.

Although the metastable state predicted by TBIM and EAM is not observed in the LEED experiment, the C_1 versus C_b profile exhibits a small increase for dilute bulk Pt concentration with respect to $C_b=50$ at. %. This particular behavior agrees quite well with the one expected in TBIM calculations and might be the first experimental evidence of metastability in a segregation process.

In addition to the oscillating concentration, which corresponds to a 1D chemical ordering perpendicular to the surface, 2D ordering is observed parallel to the surface. This ordering tendency, appearing as features in the LEED diffuse background, is clearly attributed to a particular atomic arrangement in the second layer which contains 50 at. % Pt and 50 at. % Ni. We conclude that, very likely, among different possibilities, a specific active site is largely predominant. This site is such that Pt atoms have only Ni first neighbors in contrast with other sites having one or two Pt first neighbors. This fact has

certainly important consequences in the context of catalysis.

Our results call for some new investigations: (i) the problem of reconstruction, in the Pt-rich region, should be studied in order to find the limit where the alloy starts to reconstruct; (ii) whether the chemisorption sites are unique has to be considered; high-resolution electron-energy-loss spectroscopy as well as thermal-desorption spectroscopy should valuably contribute; (iii) finally, diffuse LEED, extended to the alloy surfaces, could yield much information on the correlations among species in mixed layers.

ACKNOWLEDGMENTS

We are indebted to P. Beccat, G. d'Assenza, and P. Brun for their assistance and to Y. Joly for a critical reading of the manuscript. This work is part of the scientific program conducted by the Groupement Surface Rhone Alpes, France. The Laboratoire de Spectrométrie Physique is "Unité associée au Centre National de la Recherche Scientifique No. D008." The Laboratoire M. Letort is "Unité associée au Centre National de la Recherche Scientifique No. LP6851."

*Permanent address: Laboratoire M. Letort, Boîte Postale 104, 54600 Villers-les-Nancy, France

[1]Y. Gauthier, Y. Joly, R. Baudoing, and J. Rundgren, Phys. Rev. B **31**, 6216 (1985).

[2]R. Baudoing, Y. Gauthier, M. Lundberg, and J. Rundgren, J. Phys. C **19**, 2825 (1986).

[3]Y. Gauthier, R. Baudoing, Y. Joly, J. Rundgren, J. C. Bertolini, and J. Massardier, Surf. Sci. **162**, 342 (1985).

[4]J. Massardier and J. C. Bertolini, J. Catal. **90**, 358 (1984).

[5]Y. Gauthier, R. Baudoing, M. Lundberg, and J. Rundgren, Phys. Rev. B **35**, 7867 (1987).

[6]B. Legrand and G. Treglia, in *Proceedings of the Second International Conference on the Structure of Surfaces (ICSOS II),* Amsterdam, 1987, edited by J. F. van der Veen and M. A. van Hove (Springer-Verlag, Berlin, 1987) p. 197.

[7]M. Lundberg, Phys. Rev. B **36**, 4692 (1987).

[8]L. de Bersuder, Rev. Sci. Instrum. **45**, 1569 (1974).

[9]W. B. Pearson, *A Handbook of Lattice Spacings and Structures of Metals and Alloys* (Pergamon, London, 1964).

[10]C. E. Dahmani, M. C. Cadeville, J. M. Sanchez, and J. L. Moran Lopez, Phys. Rev. Lett. **55**, 1208 (1985).

[11]J. B. Pendry, *Low Energy Electron Diffraction* (Academic, London, 1974).

[12]J. Rundgren and A. Salven, J. Phys. C **9**, 3701 (1976).

[13]Y. Gauthier, R. Baudoing, Y. Joly, C. Gaubert, and J. Rundgren, J. Phys. C **17**, 4547 (1984).

[14]B. L. Gyorffy and G. M. Stocks, in *Electrons in Disordered Metallic Surfaces,* edited by P. Phariseau, B. L. Gyorffy, and L. Scheire (Plenum, New York, 1979).

[15]J. Philip and J. Rundgren, in *Determination of Surface Structure by LEED,* edited by P. M. Marcus and F. Jona (Plenum, New York, 1984).

[16]T. S. King and R. G. Donnelly, Surf. Sci. **141**, 417 (1984).

[17]M. Lundberg (private communication).

[18]D. Dufayard, R. Baudoing, and Y. Gauthier (unpublished).

[19]F. F. Abraham and C. R. Brundle, J. Vac. Sci. Technol. **18**, 506 (1981).

[20]B. Legrand, G. Tréglia, and F. Ducastelle (unpublished).

[21]G. Tréglia and B. Legrand, Phys. Rev. B **35**, 4338 (1987).

[22]G. Tréglia, B. Legrand, F. Ducastelle (unpublished).

[23]C. Creemers (private communication).

[24]R. Imbihl, M. P. Cox, and G. Ertl, J. Chem. Phys. **84**, 3619 (1986); S. Ladas, R. Imbihl, and G. Ertl, Surf. Sci. **197**, 163 (1988); **198**, 42 (1988).

[25]J. C. Bertolini, J. Massardier, Ph. Ruiz, and B. Tardy (unpublished).

[26]R. Baudoing, Y. Gauthier, and Y. Joly, J. Phys. C **18**, 4661 (1985).

[27]P. Fery, W. Moritz, and D. Wolf, Phys. Rev. B **38**, 7275 (1988).

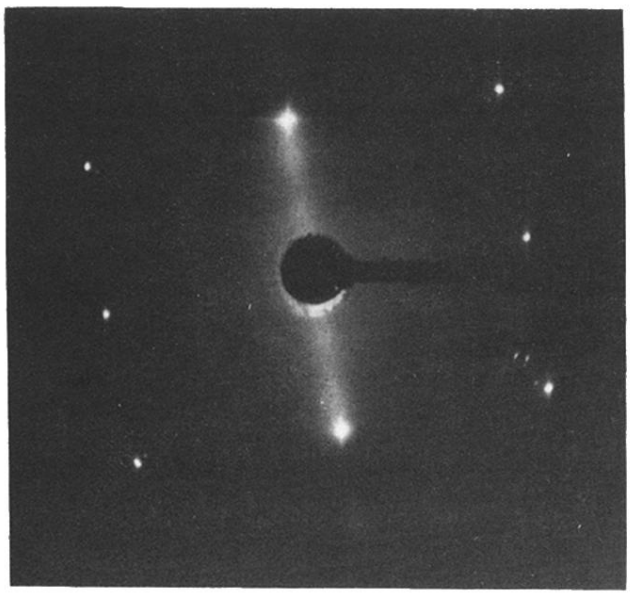

FIG. 1. Typical LEED pattern from $Pt_{10}Ni_{90}(110)$ close to normal incidence (see text). The spots correspond to the bulk periodicity. Additional weak streaks are visible along the [100] direction. (The small spurious satellites are artifacts due to reflection in the glass screen.)